Neonatal isolation augments social dominance by altering actin dynamics in the medial prefrontal cortex

Hirobumi Tada[a], Tomoyuki Miyazaki[a], Kiwamu Takemoto[a,b], Kenkichi Takase[c], Susumu Jitsuki[a], Waki Nakajima[a], Mayu Koide[a], Naoko Yamamoto[a], Kasane Komiya[a], Kumiko Suyama[a], Akane Sano[a], Akiko Taguchi[d], and Takuya Takahashi[a,1]

[a]Department of Physiology, Yokohama City University Graduate School of Medicine, Yokohama 236-0004, Japan; [b]Precursory Research for Embryonic Science and Technology, Japan Science and Technology Agency, Saitama 332-0012, Japan; [c]Laboratory of Psychology, Jichi Medical University, Tochigi 329-0498, Japan; and [d]Department of Integrative Aging Neuroscience, National Center for Geriatrics and Gerontology, Aichi 474-8511, Japan

Edited by Bruce S. McEwen, The Rockefeller University, New York, NY, and approved September 28, 2016 (received for review April 23, 2016)

Social separation early in life can lead to the development of impaired interpersonal relationships and profound social disorders. However, the underlying cellular and molecular mechanisms involved are largely unknown. Here, we found that isolation of neonatal rats induced glucocorticoid-dependent social dominance over nonisolated control rats in juveniles from the same litter. Furthermore, neonatal isolation inactivated the actin-depolymerizing factor (ADF)/cofilin in the juvenile medial prefrontal cortex (mPFC). Isolation-induced inactivation of ADF/cofilin increased stable actin fractions at dendritic spines in the juvenile mPFC, decreasing glutamate synaptic AMPA receptors. Expression of constitutively active ADF/cofilin in the mPFC rescued the effect of isolation on social dominance. Thus, neonatal isolation affects spines in the mPFC by reducing actin dynamics, leading to altered social behavior later in life.

medial prefrontal cortex | social isolation stress | social dominance | AMPA receptor trafficking | actin dynamics

Individuals exposed early in life to social separation, one form of neglect, develop impaired interpersonal relationships, including aggressive behaviors, and, in many cases, suffer from psychiatric illness (e.g., depression, borderline personality disorder, and dissociative disorder) (1–7). Although there is evidence that functional circuits in the medial prefrontal cortex (mPFC) regulate social behaviors (8), the effect of social separation early in life on neural circuit development in the mPFC is not well understood.

Prolonged exposure to social isolation early in life can affect the formation of neural circuits in the neocortex and result in social dysfunction (2, 9, 10). Synaptic plasticity driven by experience plays central roles in establishing neural circuits (11–23). A number of studies have examined the molecular events occurring at synapses during the development of experience-driven neural plasticity. The synaptic recruitment of glutamate AMPA receptors (AMPARs) is a crucial mechanism underlying this process (11, 13–19, 24–27). We recently showed that neonatal social isolation disrupts the experience-driven synaptic delivery of AMPARs in the developing rat barrel cortex and results in defective sensory processing and altered behaviors (9, 10). Other recent studies also suggest that dysfunction of glutamatergic neurotransmission is considered to be a core feature of stress-related mental illness (28, 29).

Actin is present at high concentrations in postsynaptic spines (30–32). It is the primary cytoskeletal component of synapses and also regulates the assembly of postsynaptic proteins, including AMPARs (30, 31, 33–35). A number of proteins regulate the dynamics of actin. The actin-depolymerizing factor (ADF)/cofilin family of actin-binding proteins is essential for actin filament turnover (36). Notably, ADF/cofilin mediates AMPAR trafficking during synaptic plasticity, demonstrating the importance of actin dynamics for AMPAR delivery (33).

Social dominance is crucial for the organization of social structure (37). Here, we found that isolation of neonatal rats induced social dominance over nonisolated control animals in juveniles of the same litter. This behavioral alteration was dependent on the activation of glucocorticoid signaling. Furthermore, neonatal isolation inactivated ADF/cofilin in the juvenile mPFC. Isolation-induced inactivation of ADF/cofilin resulted in the reduction of synaptic AMPAR contents correlated with the accumulation of stable actin fractions at dendritic spines in the juvenile mPFC. The expression of constitutively active ADF/cofilin in the mPFC rescued the isolation-induced effect on social dominance. Thus, neonatal isolation affects spines in the mPFC by reducing actin dynamics with ADF/cofilin inactivation, leading to altered social behavior later in life.

Results

Neonatal Isolation Enhances Social Dominance. To investigate the effect of early social isolation on social behavior, we used a rat model of neonatal isolation and assessed its effects on social dominance. Neonatal pups were isolated from their mother and other siblings for 6 h/d from postnatal day (P) 7 to P11. No significant difference in the maternal behavior (carry, licking, arched back, blanket, passive, and off) of dams between isolated and nonisolated pups was observed at each time point [0900, 1100, 1400, 1630 (just after return to mother), and 1900 hours] (Fig. S1). The pups were then maintained under normal conditions, and at 4 wk of age (juvenile age) their social behaviors were assessed using a social dominance tube test (Fig. 1*A*), which

Significance

Social separation early in life can lead to the development of impaired interpersonal relationships and profound social disorders. However, the underlying cellular and molecular mechanisms involved are largely unknown. In a rat model of neonatal isolation, we examined social dominance in juveniles. We further investigated the relationship between actin dynamics and glutamate synaptic AMPA receptor delivery in spines of the medial prefrontal cortex (mPFC) of isolated animals. Here, we report that neonatal isolation alters spines in the mPFC by reducing actin dynamics, leading to the decrease of synaptic AMPA receptor delivery and altered social behavior later in life. Our study provides molecular and cellular mechanisms underlying the influence of social separation early in life on later social behaviors.

Author contributions: H.T. and T.T. designed research; H.T., T.M., K. Takase, M.K., N.Y., K.K., and K.S. performed research; K. Takemoto, S.J., W.N., A.S., and A.T. contributed new reagents/analytic tools; and H.T. and T.T. wrote the paper.

The authors declare no conflict of interest.

This article is a PNAS Direct Submission.

Freely available online through the PNAS open access option.

[1]To whom correspondence should be addressed. Email: takahast@yokohama-cu.ac.jp.

This article contains supporting information online at www.pnas.org/lookup/suppl/doi:10.1073/pnas.1606351113/-/DCSupplemental.

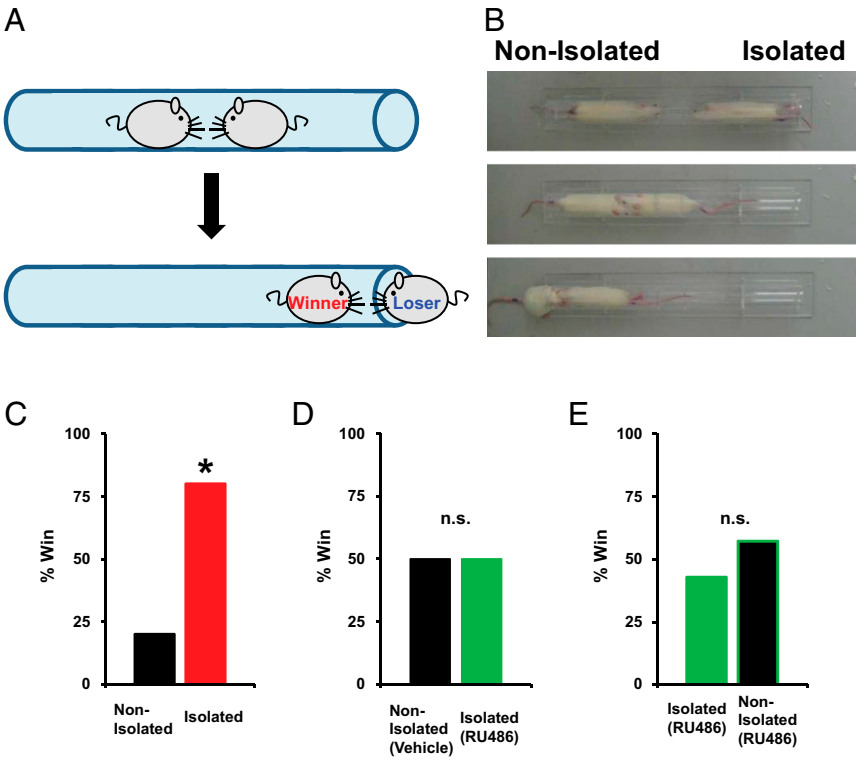

Fig. 1. Social isolation enhances social dominance. (*A*) Schematic of the tube test. In this example, the left rat pushed the right rat out of the Plexiglas tube, and the left rat was declared the winner. (*B*) Captured video images from a representative match. From top to bottom, the beginning to the end of the match is sequentially indicated. (*C*) Results of a social dominance tube test. Percentage of wins in the matches between socially isolated and nonisolated rats (10 matches). (*D*) Results of social dominance tube test between socially isolated rats treated with RU486 and nonisolated rats treated with vehicle (12 matches). (*E*) Results of social dominance tube test between socially isolated rats treated with RU486 and nonisolated rats treated with RU486 (seven matches). $*P < 0.05$ (χ^2 test).

measures social dominance or aggressive tendencies without allowing the animals to injure one another. The aggressive behaviors of two rats are analyzed during a brief pairing in a tube-shaped chamber (Fig. 1*B*). The more socially dominant rats push the counterpart rat all the way to the end of the tube. We found that neonatally isolated rats were more socially dominant compared with their nonisolated littermates [Fig. 1*C*; isolated rats won 8 of 10 matches against nonisolated rats (80%)]. In contrast to the increased social dominance, isolated rats showed no changes in body weight and locomotive activities in the open field (Fig. S2*A*). Further, we detected no significant difference in the latency of movement in the tube between isolated and nonisolated rat during eight training trials on each of two successive days (Fig. S3). We examined two additional dominance tests. Isolation increased rats' dominance in a food-competition situation relative to nonisolation (time of occupied food) (Fig. S4*A*). We also performed an agonistic behavior test. We found that neonatally isolated rats exhibited an increased number of offensive behaviors toward nonisolated rats (Fig. S4*B*). These results suggested that neonatal isolation increased social dominance.

We have previously shown that neonatal social isolation activates glucocorticoid signaling such that the duration of social isolation and the serum corticosterone levels are positively correlated (9). To determine whether the activation of glucocorticoid signaling mediates isolation-induced social dominance we treated pups undergoing social isolation with RU486, a glucocorticoid receptor antagonist, and then assessed social dominance at 4 wk of age. We found that treatment with RU486 during isolation prevented the enhancement of social dominance [Fig. 1*D*; isolated rats treated with RU486 won 6 of 12 matches against vehicle-treated nonisolated rats (50%)], suggesting that the isolation-induced enhancement of social dominance is mediated by the activation of glucocorticoid signaling. We detected no significant difference in social dominance (tube test) between isolated rats treated with RU486 and nonisolated rats treated with RU486 [Fig. 1*E*; nonisolated RU486-treated rats won four of seven matches against isolated rats treated with RU486 (57%)]. The application of RU486 did not affect body weight and open field locomotor activity (Fig. S2*B*).

Neonatal Isolation Decreases Synaptic AMPAR Contents in the Juvenile mPFC. To investigate the molecular and cellular mechanisms underlying neonatal isolation-enhanced social dominance we focused on the development of neural circuits in the mPFC, because this area is critical for regulating social behavior (8). Thus, we analyzed whether neonatal isolation affects synaptic AMPAR levels in the juvenile mPFC. We isolated pups as described above and then maintained them in a normal environment until 4 wk of age, at which time acute brain slices were prepared. The brain slices were subjected to electrophysiological recording to observe the miniature excitatory postsynaptic currents (mEPSCs) of layer 2/3 pyramidal neurons. There were no significant differences in the electrophysiological properties of neurons between isolated and nonisolated rats (Fig. S5). We found that the mEPSCs of socially isolated animals exhibited reduced amplitudes compared with those of nonisolated control rats (Fig. 2*A*), similar to the previous finding in the developing barrel cortex (9). Consistent with these electrophysiological results, we detected reduced levels of GluA1 in the postsynaptic density (PSD) fraction of the mPFC from isolated animals compared with nonisolated animals (Fig. S6*A*). Further, no significant difference in the amplitude and frequency of the miniature

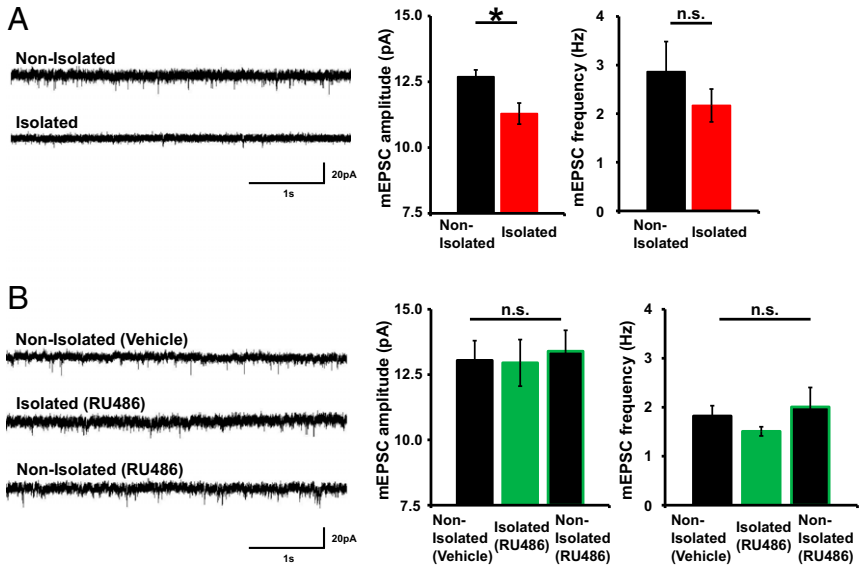

Fig. 2. Social isolation alters glutamatergic transmission in the mPFC by glucocorticoid activation. (*A*) (*Left*) Representative mEPSC traces obtained from layer 2/3 pyramidal neurons in the mPFC of socially isolated or nonisolated juvenile rats. (*Right*) Graphs depicting the average mEPSC amplitude and frequency ($n = 6$ neurons nonisolated and $n = 10$ neurons isolated). (*B*) (*Left*) Representative mEPSC traces obtained from layer 2/3 pyramidal neurons in the mPFC of RU486-treated socially isolated rats, vehicle-treated controls, and RU486 treated controls. (*Right*) Graphs depicting the average mEPSC amplitude and frequency ($n = 9$ neurons nonisolated with vehicle, $n = 8$ neurons isolated with RU486, and $n = 6$ neurons nonisolated with RU486) [amplitude, ANOVA $F_{(2,\ 20)} = 0.070$; frequency, ANOVA $F_{(2,\ 20)} = 1.072$]. *$P < 0.05$ (*A*, unpaired Student's *t* test and *B*, ANOVA post hoc Fisher's PLSD test). Error bars represent SEM. n.s., not statistically significant.

inhibitory postsynaptic current (mIPSC) and the NMDA receptor-mediated mEPSC was observed between isolated and nonisolated rat mPFC (Fig. S6 *B* and *C*). Thus, early social isolation decreased synaptic AMPAR levels in the juvenile mPFC. The injection of RU486 during isolation prevented the reduction of mEPSC amplitudes in the juvenile mPFC, indicating that this effect was dependent on the activation of glucocorticoid signaling during neonatal social isolation (Fig. 2*B*). We found no significant difference in the mEPSC amplitude and frequency among nonisolated rats treated with either RU486 or vehicle, or isolated rats treated with RU486 (Fig. 2*B*). This result is consistent with other studies demonstrating the glucocorticoid signaling dependence of stress-induced alterations in glutamate transmission (9, 28).

ADF/Cofilin Is Inactivated in the Juvenile mPFC of Neonatally Isolated Rats. ADF/cofilin mediates AMPAR trafficking during synaptic plasticity (33). Therefore, we investigated the possibility that alterations in ADF/cofilin mediate the decrease of synaptic AMPAR levels in the juvenile mPFCs of socially isolated animals. ADF/cofilin is inactivated by phosphorylation of its serine-3 (Ser3) residue and activated by Ser3's dephosphorylation (33). To determine whether neonatal isolation alters ADF/cofilin activity, we analyzed Ser3 phosphorylation levels in ADF/cofilin expressed in the juvenile mPFC of socially isolated and control animals. Synaptoneurosome fractions were isolated from the mPFC of the two treatment groups at 4 wk of age, and the phosphorylation of ADF/cofilin Ser3 was quantified. We detected elevated ADF/cofilin Ser3 phosphorylation in the socially isolated rats compared with control animals (Fig. 3*A*), which was glucocorticoid-dependent, because treatment with RU486 during isolation prevented the increased Ser3 phosphorylation (Fig. 3*C*). We found no significant difference in the phosphorylation of ADF/cofilin between RU486-treated isolated rats and nonisolated rat treated with RU486 (Fig. 3*D*). These results suggest that neonatal isolation inactivated ADF/cofilin via glucocorticoid activation and that this inactivation is maintained until the juvenile age. Furthermore, we found increased activation of LIM kinase (LIMK; this kinase is activated when its threonine-508 is phosphorylated, we detected increased phosphorylation of threonine-508 of the mPFC of isolated animals compared with nonisolated animals), which phosphorylates ADF/cofilin Ser3, in the socially isolated compared with control rats (Fig. 3*B*). We hypothesized that neonatal isolation stress-induced inactivation of ADF/cofilin mediated the decrease in synaptic AMPARs in the mPFC. To test this hypothesis, we introduced expression vectors for red fluorescent protein (RFP)-ADF/cofilin Ser3A (Ser3 is mutated to alanine, a constitutive active form of ADF/cofilin) or RFP alone into the mPFC by in utero electroporation and isolated animals, as described above. We then prepared acute brain slices from juveniles at 4 wk of age and recorded mEPSCs from layer 2/3 pyramidal neurons in the mPFC. We found that the amplitude of the mEPSCs from socially isolated animals expressing RFP-ADF/cofilin Ser3A was significantly greater than that of socially isolated animals expressing RFP (Fig. 3*E*) and was comparable to that of nonisolated control animals. This indicated that the isolation-induced decrease in synaptic AMPARs was mediated by ADF/cofilin inactivation (compare Figs. 2*A* and 3*E*).

Neonatal Isolation Increases the Stable Actin Fraction at Spines of the Juvenile mPFC. Because ADF/cofilin regulates actin dynamics (36), we next asked whether isolation stress alters actin dynamics at layer 2/3 spines in the juvenile mPFC. We introduced an expression vector for GFP-tagged actin, using in utero electroporation to deliver it into the cortical area that develops into the mPFC; treated pups were subjected to neonatal isolation. When the rats were 4 wk old, acute brain slices were prepared and subjected to FRAP (fluorescence recovery after photobleaching) analysis.

In this analysis, an individual spine in layer 2/3 of the mPFC was rapidly photobleached using high-intensity laser illumination with a two-photon laser-scanning microscope (excitation wavelength of 910 nm). The time course of the subsequent fluorescence recovery in the photobleached spine was used to evaluate actin dynamics. The mechanism of actin turnover involves polymerization at the barbed end and depolymerization at the pointed end (32). In the case of fluorescent proteins such as tdTomato,

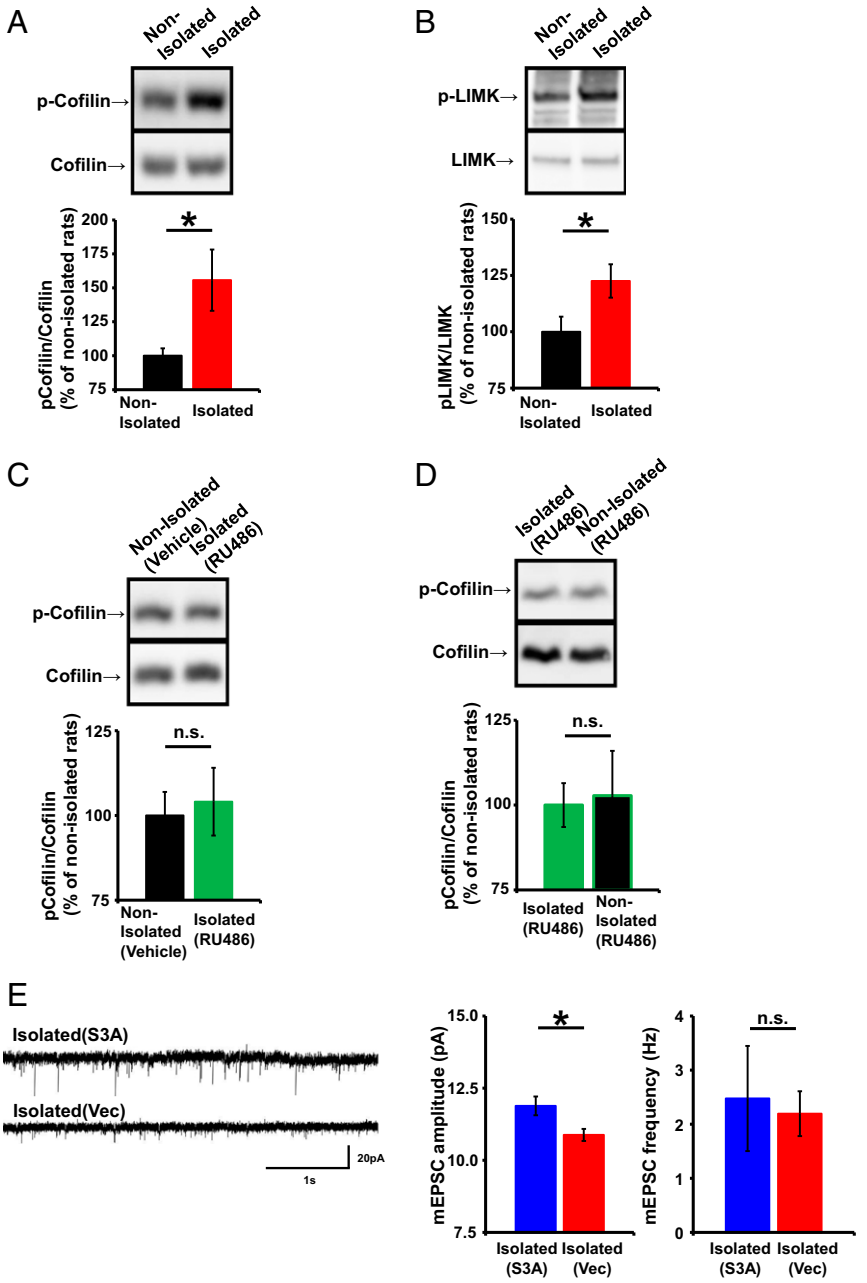

Fig. 3. Neonatal isolation inactivates ADF/cofilin in the juvenile mPFC. (*A–D*) (*Top*) Representative Western blots of synaptoneurosome fractions obtained from the mPFC of socially isolated and nonisolated rats. (*Bottom*) Graphs depicting the average ratio of phosphorylated to total ADF/cofilin (*A*, $n = 11$ rats nonisolated and 12 rats isolated; *C*, $n = 20$ rats nonisolated with vehicle and 15 rats isolated with RU486; and *D*, $n = 6$ rats isolated with RU486 and 8 rats nonisolated with RU486) and the average ratio of phosphorylated to total LIMK (*B*, $n = 17$ rats nonisolated and 15 rats isolated). (*E*) (*Left*) Representative mEPSC traces obtained from layer 2/3 pyramidal neurons in the mPFC of socially isolated animals expressing RFP-S3A or RFP. (*Right*) Graphs depicting the average mEPSC amplitude and frequency ($n = 11$ neurons isolated with S3A and 6 neurons isolated with vector). *$P < 0.05$ (unpaired Student's *t* test). Error bars represent SEM. n.s., not statistically significant.

which diffuse freely, the fluorescence levels are rapidly and completely recovered (Fig. S7*A*). However, if a portion of the protein is bound to scaffolding proteins, the fluorescence recovery is partial, and there will be an unrecoverable fraction. The presence of stable actin filaments with reduced turnover also results in an increased unrecoverable fraction during FRAP analysis.

We detected a significant increase in the unrecoverable fraction of GFP-actin in the photobleached spines obtained from socially isolated animals compared with control nonisolated animals (Fig. 4 *A* and *B*), indicating that early social isolation increased the stable immobilized fraction of actin. Notably, we detected no difference in the time constant (τ) of fluorescence recovery (Fig. 4*B*) and spine size (Fig. S7*B*) between isolated and nonisolated animals. We also analyzed the spine shape in the mPFC of either isolated or nonisolated animals with Golgi staining. The number of mushroom-type, mature spines was greater in the isolated rat mPFC than in the nonisolated rat mPFC. Furthermore, the number of immature, stubby-type spines was greater in the nonisolated rat mPFC than in that of isolated rat. No significant difference in the number of total spines and filopodia spines was observed between isolated and nonisolated rat mPFC (Fig. S8). These findings suggested that

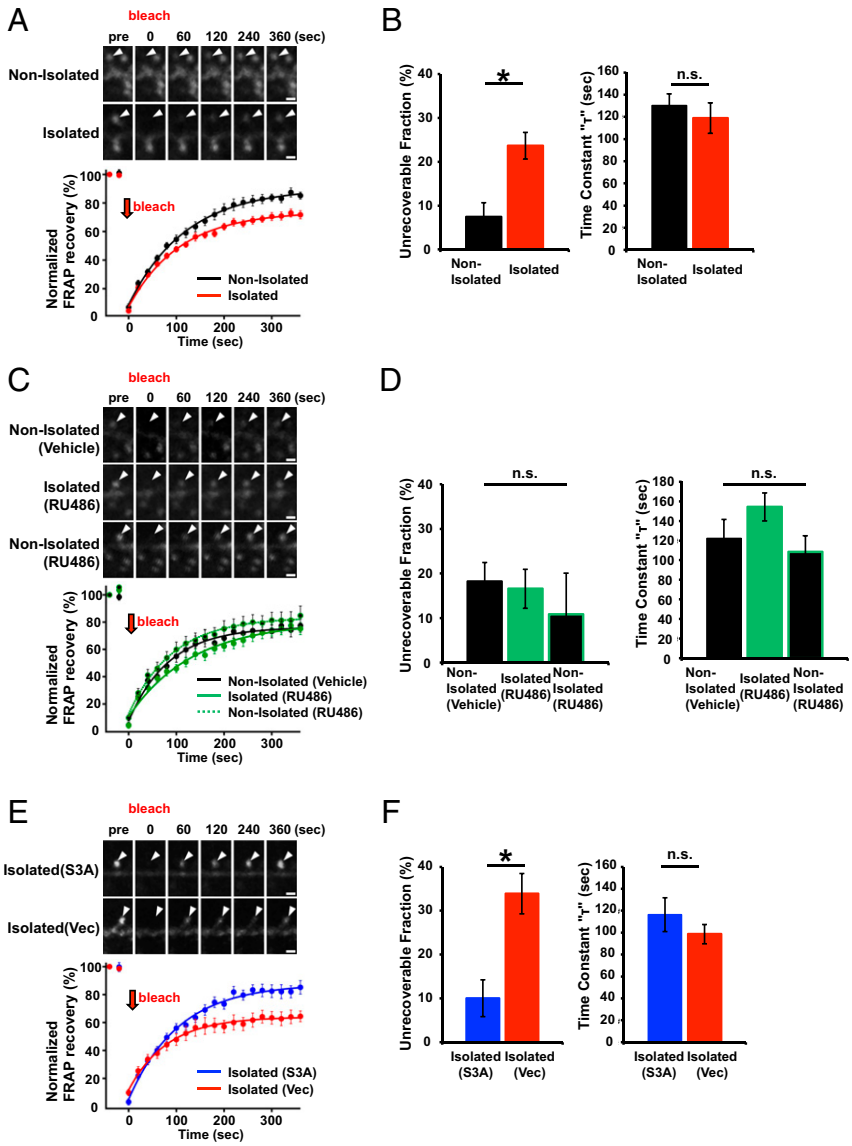

Fig. 4. ADF/cofilin inactivation mediates the increased stable actin fraction at spines in the juvenile mPFC of socially isolated rats. (*A* and *C*) FRAP analysis of GFP-actin in spines of the mPFC layer 2/3 neurons of socially isolated and nonisolated rats. Representative images and graphs depict the average GFP-actin signals before and after spine photobleaching. (*B* and *D*) Recovery time constants and quantification of the unrecoverable fractions of the FRAP samples analyzed in *A* (n = 15 spines nonisolated and 35 spines isolated) and *C* (n = 20 spines nonisolated with vehicle, 22 spines isolated with RU486, and 16 spines nonisolated with RU486) [unrecoverable fraction, ANOVA $F_{(2,\ 55)} = 1.959$; time constant, ANOVA $F_{(2,\ 55)} = 0.393$]. (*E*) FRAP analysis as in *A* for socially isolated rats expressing GFP-actin with RFP-S3A or RFP. (*F*) Recovery time constants and quantification of the unrecoverable fraction of the FRAP samples analyzed in *E* (n = 11 spines isolated with S3A and 10 spines isolated with vector). Arrowheads: dendritic spines. *$P < 0.05$ (*B* and *F*, unpaired Student's t test; *D*, ANOVA post hoc Fisher's PLSD test). Error bars represent SEM. n.s., not statistically significant. (Scale bars: 1 μm.)

there may be two fractions of actin filaments: one that was unaffected by isolation and exhibited normal turnover and another that was altered by isolation and ceased dynamic turnover, resulting in the increased unrecoverable fraction after photobleaching without changing spine size. The increase in the stable immobilized fraction of actin in response to neonatal isolation was glucocorticoid signaling-dependent, because the application of RU486 during neonatal isolation blocked this effect (Fig. 4 *C* and *D*; no significant difference in the actin dynamics was observed among nonisolated with vehicle, isolated with RU486, and nonisolated rats with RU486).

We next investigated whether ADF/cofilin inactivation mediated the isolation-induced increase in stable actin. We introduced expression vectors for GFP-actin and the RFP-tagged ADF/cofilin Ser3A constitutive active mutant by in utero electroporation (33) and assessed the fraction of stable GFP-actin in the mPFC of socially isolated and control animals by FRAP analysis. The unrecoverable fraction of GFP-actin in the socially isolated animals expressing Ser3A was significantly reduced compared with that of socially isolated animals treated with control vector (Fig. 4 *E* and *F*) and was comparable to that of the nonisolated control animals (compare Fig. 4 *B* and *F*). These results indicate that the isolation-induced increase in the stable actin fraction is mediated by ADF/cofilin inactivation. The level of endogenous total ADF/cofilin was comparable between RFP-tagged constitutively active ADF/cofilin-transfected and untransfected neurons (Fig. S9*A*). To assess the effect of the overexpression of the constitutively active ADF/cofilin on spine morphology we cotransfected GFP and RFP-tagged ADF/cofilin Ser3A in the mPFC of the normal animal with in utero electroporation. At 4 wk of age, we prepared acute

brain slices and examined the spine morphology by the observation of GFP (38–41). No significant differences were observed in the spine shape and size of the mPFC neurons with overexpression of constitutively active ADF/cofilin (Fig. S9 *B*, *C*, and *D*). In addition, no significant differences were observed in the basal dendrite length and branches of the mPFC neurons with overexpression of constitutively active ADF/cofilin (Fig. S9 *E* and *F*).

The Isolation-Induced Increase in Stable Actin Interferes with the Synaptic Delivery of AMPARs. To investigate the relationship between the increased stable actin fraction and the decreased synaptic AMPAR levels in the socially isolated animals we cointroduced expression vectors for superecliptic pHluorin (SEP) fused to the N terminus of GluA1 and tdTomato-tagged actin into the mPFC by in utero electroporation. We then isolated rat pups as described above and prepared acute brain slices at 4 wk of age. The expression of SEP-GluA1 is selectively detected at the cell surface due to the strong fluorescence of SEP at pH 7 and above, and its fluorescence is diminished when it is localized to acidic secretory compartments. We performed FRAP analysis on the brain slices to evaluate the tdTomato-actin dynamics at individual spines at layer 2/3 of the mPFC. We then chemically induced long-term potentiation (cLTP) by briefly exposing the slices to the potassium channel blocker tetraethylammonium (TEA) (33) 90 min after FRAP analysis. mEPSC amplitude was increased in slices obtained from the control nonisolated animals by TEA cLTP induction but not in those from the socially isolated animals (Fig. S10). Consistent with this finding, chemically-induced LTP increased the surface expression of GluA1 in the spines of the control animals but not in those of the socially isolated animals (Fig. 5 *A* and *B*). Notably, we found a negative correlation between the amount of stable

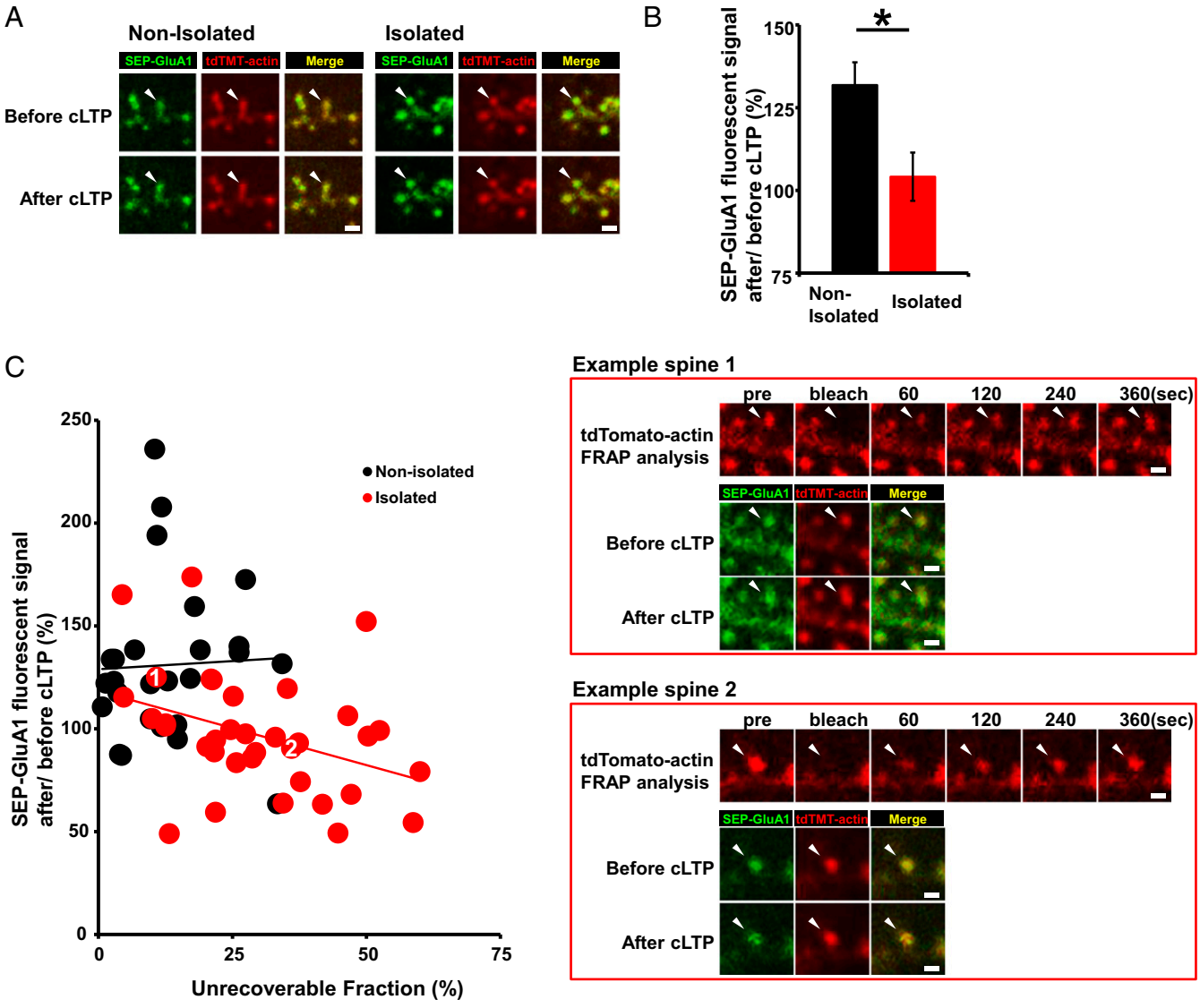

Fig. 5. The isolation-induced increase in stable actin interferes with the synaptic delivery of AMPARs. (*A*) Representative images showing SEP-GluA1 and tdTomato-actin fluorescence on spines before and after TEA treatment in the mPFC of socially isolated or nonisolated rats. (*B*) Quantification of changes in the SEP-GluA1 spine/ dendrite ratio after TEA treatment ($n = 38$ spines nonisolated and 45 spines isolated). (*C*) Two representative images. The first image shows a low unrecoverable actin fraction and a chemical LTP-induced increase in surface SEP-GluA1 (Example spine 1); the second image shows high unrecoverable actin and no LTP-induced increase in surface SEP-GluA1 (Example spine 2). The scatter plot shows the change in SEP-GluA1 intensity (presented as spine/ dendrite ratio) after TEA treatment versus the unrecoverable fraction of tdTomato-actin at individual spines. ($n = 35$ spines isolated: $r = 0.371$, $P < 0.05$; $n = 26$ spines nonisolated: $r = -0.41$, $P > 0.5$). Arrowheads indicate dendritic spines. *$P < 0.05$ (unpaired Student's t test). Error bars represent SEM. (Scale bars: 1 μm.)

actin and the LTP-induced increase in surface GluA1 at individual spines from the socially isolated animals but not from control rats (Fig. 5*C*). These findings suggest that the isolation-induced increase in stable actin interferes with the synaptic delivery of AMPARs.

ADF/Cofilin Inactivation Mediates Isolation-Induced Enhancement of Social Dominance. Next, we evaluated the relationship of the isolation-induced cellular and molecular events at spines to the changes in social dominance. We injected lentivirus expressing ADF/cofilin Ser3A-IRES-Venus or IRES-Venus into layer 2/3 of the mPFC of socially isolated rats at the juvenile age (Fig. 6*A*). To characterize the infected cells, we performed immunohistological staining of the infected area using either an anti-CaMKII or anti-GABA antibody for pyramidal neurons or interneurons, respectively. The majority of infected neurons were CaMKII-positive pyramidal neurons, whereas only a small fraction consisted of GABA-positive interneurons (Fig. S11). Notably, the ADF/cofilin Ser3A-expressing, socially isolated rats exhibited significantly less social dominance than the control vector-treated, socially isolated animals and exhibited social dominance comparable to that of vector-expressing, nonisolated animals [Fig. 6 *B* and *C*; isolated rats with S3A (mPFC) won two of eight matches against isolated rats with vector (mPFC) (25%) and won five of nine matches against nonisolated rats with vector (mPFC) (55%)], suggesting that the ADF/cofilin inactivation in the mPFC of socially isolated animals was responsible for their increased social dominance. Injection of the same amount of ADF/cofilin Ser3A virus into the M2 motor cortex had no effect on social dominance, thus suggesting that the effect was mPFC-specific [Fig. 6*D*; isolated rats with S3A (M2) won five of six matches against nonisolated rats with vector (M2) (83%)]. These data indicate that the isolation-induced inactivation of ADF/cofilin increases the stable fraction of actin, leading to decreased synaptic AMPAR levels at spines of the mPFC and the enhancement of social dominance.

Discussion

Human individuals who experienced childhood social separation, one form of neglect, tend to exhibit aggressive behaviors and impaired interactions within groups (2, 6, 7), which may result from an increased fear of other people (42). Notably, such individuals exhibit a reduced prefrontal cortical volume, suggesting that its impairment may underlie their aggressive behaviors (2). Here, we showed that rats experiencing neonatal isolation subsequently exhibited increased social dominance over nonisolated controls in the same litter, which may be due to enhanced aggression similarly to human patients exposed to early neglect such as social separation. Our mechanistic studies indicate that the neonatal social isolation-induced inactivation of ADF/cofilin results in the decrease of synaptic AMPAR contents via increased stable actin fractions at spines of the mPFC, leading to enhanced social dominance. Thus, our study reveals a molecular and cellular mechanism that underlies the alteration of social behavior in animals exposed to neonatal isolation, and that may also underlie the enhanced aggressiveness observed in people exposed to early neglect.

Previous studies reported that stress-induced alterations such as synaptic transmission and neuronal cell morphology in the nervous system are glucocorticoid-dependent (9, 10, 28, 43). Furthermore, human studies have demonstrated the importance of glucocorticoid signaling in stress-related mental disorders (44–46). In this study we found that neonatal isolation stress increased the stable fraction of actin, which is glucocorticoid-dependent. Thus, we added a new molecular alteration dependent on stress-induced glucocorticoid activation. Because actin dynamics are known to be crucial for a variety of synaptic functions (30), the altered actin dynamics at the spines in the juvenile mPFC of neonatally isolated animals could explain stress-induced neocortical dysfunction.

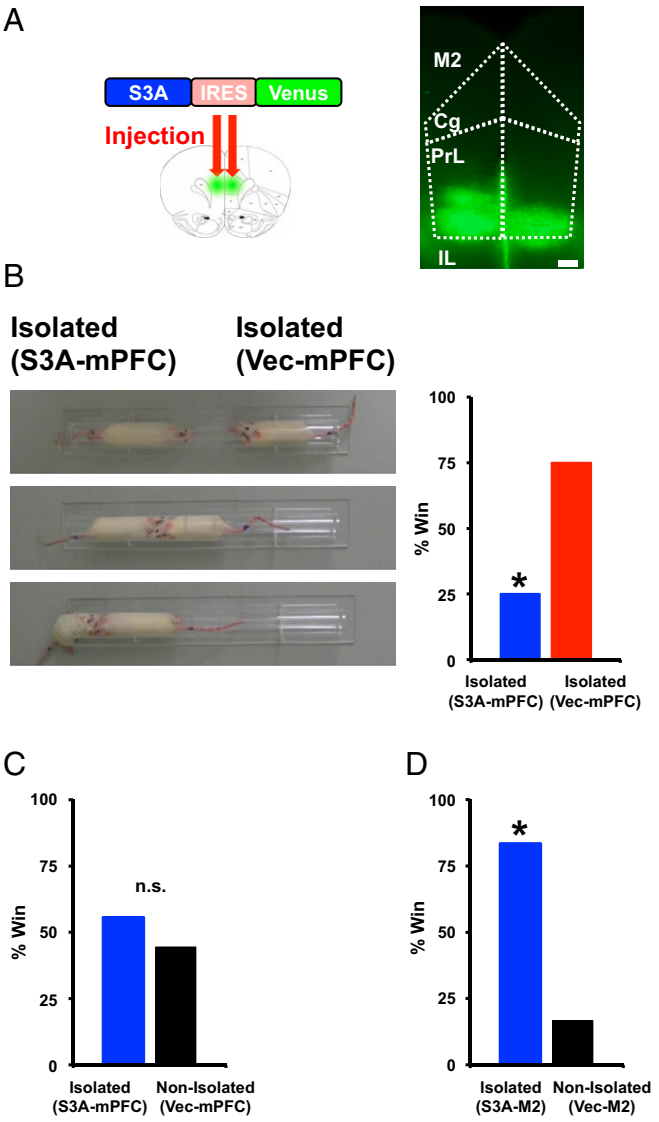

Fig. 6. Activation of ADF/cofilin in the mPFC suppresses the enhancement of social dominance in socially isolated rats. (*A*) Example of brain slices taken from an animal injected with Lenti-S3A-IRES-Venus. Subregion boundaries are indicated with dotted lines. (Cg, cingulate cortex; IL, infralimbic cortex; M2, secondary motor cortex; PrL, prelimbic cortex). (Scale bar, 300 μm.) (*B*) Social dominance tube test of socially isolated rats with mPFC injection of ADF/cofilin S3A (S3A-mPFC). (*Left*) Captured video images from a representative match. From top to bottom, the beginning to the end of the match is sequentially indicated. The socially isolated rat expressing S3A (mPFC) was pushed out by the socially isolated rat expressing vector in the mPFC (Vec-mPFC). (*Right*) Percentage of wins in the matches between socially isolated rats expressing S3A (mPFC) and vector (mPFC) (eight matches). (*C*) Social dominance tube test between socially isolated rats expressing S3A (mPFC) and nonisolated rats expressing vector (mPFC). Isolated rats (S3A-mPFC) exhibited social dominance comparable to that of nonisolated animals (vector-mPFC) (nine matches), (*D*) but not rats with other brain area, M2 motor cortex, injection (six matches). *$P < 0.05$ (χ^2 test, *B*, *C*, and *D*). n.s., not statistically significant.

The question regarding the function of the "stable actin fraction" remains, however. If the intense light-treated "nonfluorescent" GFP-actin at spines is fully replaced by "fluorescent" GFP-actin in the FRAP experiment, the bleached fluorescence should be fully recovered as a fluorescent protein alone (Fig. S7*A*). However, we found that the fluorescence recovery was partial at spines in the juvenile mPFC of neonatally isolated animals. In addition,

the increase of the stable actin fraction in isolated animals was mediated by the inactivation of ADF/cofilin, which is required for dynamic actin turnover. Thus, the increased stable actin fraction could be due to the decrease of the actin dynamics, and the stable actin fraction might be the actin fibers with reduced dynamics. Indeed, a negative correlation was found between the chemical LTP-induced increase of the surface presentation of GluA1 and the amount of the stable actin fraction at spines of isolated animals but not of nonisolated animals. Although it remains to be determined whether the reduced dynamic actin is the increased fraction of stable actin, the stable actin fraction could be interfering with synaptic AMPAR delivery.

A recent elegant study showed that higher synaptic efficacy in the mPFC results in the higher social ranking of rodents housed in a normal environment (8). This apparent discrepancy could be due to the malfunction of multiple brain areas in rats exposed to social isolation early in life (9, 10, 47). It will be interesting to determine how the alteration of neuronal function across multiple areas following neonatal isolation affects mPFC-mediated effects on social dominance. A previous report studying the limbic system exhibited that repeated social defeat chronic stress reduced expression of RAC1, which could lead to up-regulation of ADF/cofilin activity (38). This opposite effect of chronic stress on ADF/cofilin activity between the neocortex and the limbic system could be the underlying mechanism of altered social behaviors of socially isolated rats. That is, the balance of the molecular and cellular actions between the neocortex and the limbic system might be crucial for expression of social behaviors.

Methods and Materials

Animals and Neonatal Social Isolation. Sprague-Dawley (SD) rats (Charles River Laboratories) in multiple colonies that each contained five males and five females were used. Rats were housed in plastic Ekon cages and maintained on a 14-h light/10-h dark cycle (full light at 0500 hours and full darkness at 1900 hours). The temperature and humidity were held constant at 22 °C ± 1 °C and 55 ± 5%, respectively. Food and water were provided for ad libitum consumption. Procedures were performed in strict compliance with the animal use and care guidelines of Yokohama City University.

For the neonatal social isolation experiments, three male pups were isolated from their mother and siblings for 6 h/d, from 1000–1600 hours, from P7 to P11. During the isolation period, each male pup was placed alone in a smaller cage, with a heating pad at 35 °C, in an adjacent room.

Social Dominance Tube Test. Animal social dominance was tested as previously described (8, 48) in a transparent Plexiglas tube measuring 45 cm in length and 4 cm in (inside) diameter, a size just sufficient to permit one juvenile rat to pass through without reversing direction. For training, each rat was released at alternating ends of the tube and allowed to run through the tube. Each animal was given eight training trials on each of two successive days. For the social dominance test, animals were placed at opposite ends of the tube and released. A subject was declared the "winner" when its opponent backed out of the tube. The maximum test time was set to 2 min.

Drug Treatment. Systemically administered drugs were injected s.c. RU486 (8 μg/g of body weight; Sigma-Aldrich) was injected twice a day during the neonatal isolation period.

Electrophysiology. Rats were anesthetized with an isoflurane–oxygen mixture, and the brain was removed. The brain was quickly transferred into ice-cold dissection buffer gassed with 5% (vol/vol) CO2/95% (vol/vol) O2 as described previously (9). Coronal brain slices were cut (350 μm; Leica VT1000) in dissection buffer. The slices were then incubated in artificial cerebrospinal fluid (ACSF) as described previously (9).

Patch recording pipettes (3–7 MΩ) were filled with intracellular solution as described previously (9, 49, 50). To record the mEPSC or mIPSC from the PrL (prelimbic cortex) of the mPFC, the recording chamber was perfused with ACSF with 0.5 μM TTX and low magnesium (1 mM), containing 100 μM picrotoxin (for mEPSC) or 10 μM NBQX (for mIPSC). For recording NMDA-mEPSCs, the recording chamber was perfused with ACSF with zero magnesium, containing 0.5 μM TTX, 0.1 mM picrotoxin, and 10 μM NBQX. The mEPSCs, mIPSCs, or NMDA-mEPSCs were detected and analyzed using the Mini Analysis Program 6.0.7 (Synaptosoft).

Western Blotting. mPFC samples were rapidly dissected and stored at −80 °C. Synaptoneurosome fractions were prepared as previously described (9). Frozen samples were homogenized in ice-cold homogenization buffer (10 mM Hepes, 1.0 mM EDTA, 2.0 mM EGTA, 0.5 mM DTT, 0.1 mM PMSF, 10 mg/L leupeptin, and 100 nM microcystin). The tissue was homogenized in a glass/glass tissue homogenizer, and the homogenates were passed through two 100-μm-pore nylon mesh filters, and then through a 5-μm-pore filter. The filtered homogenates were centrifuged at 3,600 × *g* for 10 min at 4 °C. The resulting pellets were resuspended in 100 μL of boiling homogenization buffer with 1% SDS, followed by immunoblotting. The signal intensity of each band was measured by MultiGauge (Fujifilm). The net signal was obtained by subtracting the background signal obtained from the region adjacent to the band.

Constructs. GFP-actin and tdTomato-actin were PCR-amplified and subcloned into the pCAGGS-EX and pEF-BOS vectors, respectively. pCALNL-GluA1 and pCAG-ERT2CreERT were gifts from R. Malinow, University of California, San Diego, La Jolla, CA. The cofilin Ser3A cDNA-mRFP construct was a gift from J. Zheng, Emory University School of Medicine, Atlanta. The cofilin Ser3A cDNA was PCR-amplified and subcloned into the pEF-BOS and flap-Ub promoter-IRES-Venus-WRE vectors.

In Utero Electroporation of mPFC Neurons. Layer 2/3 progenitor cells were transfected by in utero electroporation. E17-timed pregnant SD rats (Charles River Laboratories) were anesthetized with an isoflurane–oxygen mixture. Approximately 0.5 mL of DNA solution containing fast green was pressure-injected by mouth through a pulled-glass capillary tube into the left lateral ventricle of each embryo. The head of each embryo was placed between tweezer electrodes with the anode contacting the right hemisphere. Electroporation was achieved with five square pulses (duration 50 ms, frequency 5 Hz, voltage 80 V; BEX Co.).

Analysis of FRAP Data. Images were obtained using a two-photon laser-scanning microscope (FV-1000MPE; Olympus) with a water immersion objective (25× 1.05 N.A.; Olympus). FRAP analysis was performed using a macro function of the stimulus setting menu in the Fluoview software, to control sequential image acquisition and the emission of a photobleaching laser pulse to the ROI (region of interest). A single dendritic spine of a layer 2/3 neuron in the rat PrL of the mPFC was set as the ROI. Two prebleaching images were acquired, and the spine fluorescence was then photobleached with a two-photon laser at 910 nm. The recovery of fluorescence was traced for an additional 6 min by acquiring images at 20-s intervals. Minimum laser power was used to prevent photobleaching during the pre- and post-bleaching stages. Background fluorescence was subtracted from the fluorescence of the target spine. The intensity of bleached spines was normalized to the baseline fluorescence and normalized to neighboring nonphotobleached spines at each time point. The GFP-actin or tdTomato-actin signals were fitted to a single exponential curve using the following equation (Igor Pro; Wavemetrics):

$$F = F_{t=\infty} + A\exp\left(-\frac{t}{\tau}\right),$$

where $F_{t=\infty}$ represents the unrecoverable fluorescence, considered to be a fixed population of fluorescent protein, and τ is the time constant for recovery.

Cre Recombinase Activation by 4-Hydroxytamoxifen. The 4-hydroxytamoxifen (4-OHT; Sigma-Aldrich) was dissolved in ethanol at 20 mg/mL and diluted with nine volumes of sesame oil (Sigma-Aldrich). Diluted 4-OHT (2 mg/mL) was intraperitoneally injected into each rat 2 d before FRAP analysis (500 μL per animal).

Chemically-Induced LTP and Imaging of SEP-GluA1. LTP induction was performed with a modified version of a previous method (33). For chemical stimulation, brain slices were incubated in ACSF at room temperature, followed by stimulation with 25 mM TEA (Sigma) in ACSF for 10 min, and finally followed by ACSF alone once more.

Images were captured before and 30 min after TEA cLTP induction using a two-photon laser-scanning microscope (FV-1000MPE; Olympus) with a water immersion objective (25× 1.05 N.A.; Olympus). SEP and tdTomato were excited at 910 nm with a Ti:sapphire laser (Mai Tai DeepSee; Spectra-Physics). Green and red fluorescent signals were separated by a set of dichroic mirrors and filters (Olympus). The SEP and tdTomato fluorescence in spines and dendrites was measured as integrated green and red fluorescence, respectively,

after background and leak subtraction. The ratio of the SEP fluorescence intensity of the spine head to the dendritic shaft was measured on manually selected spine head and dendritic shaft areas.

In Vivo Infection of mPFC or M2 Neurons. Rats were deeply anesthetized with an isoflurane–oxygen mixture. The skin overlying the skull was cut and gently pushed to the side. The anterior fontanel was identified and a region 3 mm anterior, 1.5 mm lateral was gently pierced with a dental drill. The recombinant lentivirus was pressure-injected through a pulled-glass capillary (Narishige) into the PrL of the mPFC [anteroposterior (AP), +3.0 mm; mediolateral (ML), +0.4 mm; and dorsoventral (DV), −3.0 mm to bregma) or M2 motor cortex (AP, +3.0 mm; ML, +1.5 mm; and DV, −1.0 mm to bregma). After injection, the skin was repositioned and its integrity was restored with cyanoacrylate glue. Rats were kept on a heating pad during the procedures and returned to their home cage after regaining movement.

Statistics. For comparison between means, we used the χ^2 test, unpaired Student's *t* test, ANOVA post hoc Fisher's protected least significant difference (PLSD) test, or repeated measures ANOVA. All data are expressed as the mean ± SEM.

ACKNOWLEDGMENTS. We thank our colleagues in the T.T. laboratory for help, encouragement, and advice; and Dr. R. Malinow and Dr. J. Zheng for valuable reagents. This project was supported by Special Coordination Funds for Promoting Science and Technology (T.T.) and Grants-in-Aid for Scientific Research 26290025 (to T.T.), 15K15041, and 24700382 (to H.T.) and a grant for the "Development of Biomarker Candidates for Social Behavior," carried out under the Strategic Research Program for Brain Sciences by the Ministry of Education, Culture, Sports, Science and Technology of Japan (to T.T.). This work was partially supported by the Strategic Research Program for Brain Sciences from Japan Agency for Medical Research and Development (T.T.) and the Brain Mapping by Integrated Neurotechnologies for Disease Studies (Brain/MINDS) from Japan Agency for Medical Research and Development (T.T.).

1. Hengartner MP, Ajdacic-Gross V, Rodgers S, Müller M, Rössler W (2013) Childhood adversity in association with personality disorder dimensions: New findings in an old debate. *Eur Psychiatry* 28(8):476–482.
2. Morandotti N, et al. (2013) Childhood abuse is associated with structural impairment in the ventrolateral prefrontal cortex and aggressiveness in patients with borderline personality disorder. *Psychiatry Res* 213(1):18–23.
3. Rivera-Vélez GM, González-Viruet M, Martínez-Taboas A, Pérez-Mojica D (2014) Post-traumatic stress disorder, dissociation, and neuropsychological performance in Latina victims of childhood sexual abuse. *J Child Sex Abuse* 23(1):55–73.
4. Infurna MR, et al. (2016) Associations between depression and specific childhood experiences of abuse and neglect: A meta-analysis. *J Affect Disord* 190:47–55.
5. Nemeroff CB (2016) Paradise lost: The neurobiological and clinical consequences of child abuse and neglect. *Neuron* 89(5):892–909.
6. Kotch JB, et al. (2008) Importance of early neglect for childhood aggression. *Pediatrics* 121(4):725–731.
7. Logan-Greene P, Semanchin Jones A (2015) Chronic neglect and aggression/delinquency: A longitudinal examination. *Child Abuse Negl* 45:9–20.
8. Wang F, et al. (2011) Bidirectional control of social hierarchy by synaptic efficacy in medial prefrontal cortex. *Science* 334(6056):693–697.
9. Miyazaki T, et al. (2012) Disrupted cortical function underlies behavior dysfunction due to social isolation. *J Clin Invest* 122(7):2690–2701.
10. Miyazaki T, et al. (2013) Social isolation perturbs experience-driven synaptic glutamate receptor subunit 4 delivery in the developing rat barrel cortex. *Eur J Neurosci* 37(10):1602–1609.
11. Takahashi T, Svoboda K, Malinow R (2003) Experience strengthening transmission by driving AMPA receptors into synapses. *Science* 299(5612):1585–1588.
12. Miyazaki T, et al. (2012) Developmental AMPA receptor subunit specificity during experience-driven synaptic plasticity in the rat barrel cortex. *Brain Res* 1435:1–7.
13. Clem RL, Barth A (2006) Pathway-specific trafficking of native AMPARs by in vivo experience. *Neuron* 49(5):663–670.
14. Kessels HW, Malinow R (2009) Synaptic AMPA receptor plasticity and behavior. *Neuron* 61(3):340–350.
15. Mitsushima D, Ishihara K, Sano A, Kessels HW, Takahashi T (2011) Contextual learning requires synaptic AMPA receptor delivery in the hippocampus. *Proc Natl Acad Sci USA* 108(30):12503–12508.
16. Mitsushima D, Sano A, Takahashi T (2013) A cholinergic trigger drives learning-induced plasticity at hippocampal synapses. *Nat Commun* 4:2760.
17. Rumpel S, LeDoux J, Zador A, Malinow R (2005) Postsynaptic receptor trafficking underlying a form of associative learning. *Science* 308(5718):83–88.
18. Jitsuki S, et al. (2011) Serotonin mediates cross-modal reorganization of cortical circuits. *Neuron* 69(4):780–792.
19. Lee HK, et al. (2003) Phosphorylation of the AMPA receptor GluR1 subunit is required for synaptic plasticity and retention of spatial memory. *Cell* 112(5):631–643.
20. Whitlock JR, Heynen AJ, Shuler MG, Bear MF (2006) Learning induces long-term potentiation in the hippocampus. *Science* 313(5790):1093–1097.
21. Trachtenberg JT, et al. (2002) Long-term in vivo imaging of experience-dependent synaptic plasticity in adult cortex. *Nature* 420(6917):788–794.
22. Jacob V, Petreanu L, Wright N, Svoboda K, Fox K (2012) Regular spiking and intrinsic bursting pyramidal cells show orthogonal forms of experience-dependent plasticity in layer V of barrel cortex. *Neuron* 73(2):391–404.
23. Huang S, et al. (2012) Pull-push neuromodulation of LTP and LTD enables bidirectional experience-induced synaptic scaling in visual cortex. *Neuron* 73(3):497–510.
24. Tada H, et al. (2013) Phasic synaptic incorporation of GluR2-lacking AMPA receptors at gonadotropin-releasing hormone neurons is involved in the generation of the luteinizing hormone surge in female rats. *Neuroscience* 248:664–669.
25. Tada H, et al. (2015) Estrous cycle-dependent phasic changes in the stoichiometry of hippocampal synaptic AMPA receptors in rats. *PLoS One* 10(6):e0131359.
26. Jitsuki S, et al. (2016) Nogo receptor signaling restricts adult neural plasticity by limiting synaptic AMPA receptor delivery. *Cereb Cortex* 26(1):427–439.
27. Nakajima W, Jitsuki S, Sano A, Takahashi T (2016) Sustained enhancement of lateral inhibitory circuit maintains cross modal cortical reorganization. *PLoS One* 11(2): e0149068.
28. Popoli M, Yan Z, McEwen BS, Sanacora G (2011) The stressed synapse: The impact of stress and glucocorticoids on glutamate transmission. *Nat Rev Neurosci* 13(1):22–37.
29. Yuen EY, et al. (2012) Repeated stress causes cognitive impairment by suppressing glutamate receptor expression and function in prefrontal cortex. *Neuron* 73(5):962–977.
30. Dillon C, Goda Y (2005) The actin cytoskeleton: Integrating form and function at the synapse. *Annu Rev Neurosci* 28:25–55.
31. Okamoto K, Nagai T, Miyawaki A, Hayashi Y (2004) Rapid and persistent modulation of actin dynamics regulates postsynaptic reorganization underlying bidirectional plasticity. *Nat Neurosci* 7(10):1104–1112.
32. Star EN, Kwiatkowski DJ, Murthy VN (2002) Rapid turnover of actin in dendritic spines and its regulation by activity. *Nat Neurosci* 5(3):239–246.
33. Gu J, et al. (2010) ADF/cofilin-mediated actin dynamics regulate AMPA receptor trafficking during synaptic plasticity. *Nat Neurosci* 13(10):1208–1215.
34. Okabe S (2012) Molecular dynamics of the excitatory synapse. *Adv Exp Med Biol* 970: 131–152.
35. Chen LY, Rex CS, Casale MS, Gall CM, Lynch G (2007) Changes in synaptic morphology accompany actin signaling during LTP. *J Neurosci* 27(20):5363–5372.
36. Bamburg JR, Bernstein BW (2010) Roles of ADF/cofilin in actin polymerization and beyond. *F1000 Biol Rep* 2:62.
37. Hooper PL, Kaplan HS, Boone JL (2010) A theory of leadership in human cooperative groups. *J Theor Biol* 265(4):633–646.
38. Golden SA, et al. (2013) Epigenetic regulation of RAC1 induces synaptic remodeling in stress disorders and depression. *Nat Med* 19(3):337–344.
39. Jia JM, Zhao J, Hu Z, Lindberg D, Li Z (2013) Age-dependent regulation of synaptic connections by dopamine D2 receptors. *Nat Neurosci* 16(11):1627–1636.
40. Peebles CL, et al. (2010) Arc regulates spine morphology and maintains network stability in vivo. *Proc Natl Acad Sci USA* 107(42):18173–18178.
41. Mucha M, et al. (2011) Lipocalin-2 controls neuronal excitability and anxiety by regulating dendritic spine formation and maturation. *Proc Natl Acad Sci USA* 108(45): 18436–18441.
42. Guillot PV, Chapouthier G (1996) Intermale aggression and dark/light preference in ten inbred mouse strains. *Behav Brain Res* 77(1–2):211–213.
43. Yuen EY, et al. (2011) Mechanisms for acute stress-induced enhancement of glutamatergic transmission and working memory. *Mol Psychiatry* 16(2):156–170.
44. Labonte B, et al. (2012) Differential glucocorticoid receptor exon 1(B), 1(C), and 1(H) expression and methylation in suicide completers with a history of childhood abuse. *Biol Psychiatry* 72(1):41–48.
45. McGowan PO, et al. (2009) Epigenetic regulation of the glucocorticoid receptor in human brain associates with childhood abuse. *Nat Neurosci* 12(3):342–348.
46. Anacker C, O'Donnell KJ, Meaney MJ (2014) Early life adversity and the epigenetic programming of hypothalamic-pituitary-adrenal function. *Dialogues Clin Neurosci* 16(3):321–333.
47. Makinodan M, Rosen KM, Ito S, Corfas G (2012) A critical period for social experience-dependent oligodendrocyte maturation and myelination. *Science* 337(6100): 1357–1360.
48. Lindzey G, Winston H, Manosevitz M (1961) Social dominance in inbred mouse strains. *Nature* 191:474–476.
49. Tada H, et al. (2010) Fbxo45, a novel ubiquitin ligase, regulates synaptic activity. *J Biol Chem* 285(6):3840–3849.
50. Takemoto K, et al. (2016) Optical inactivation of synaptic AMPA receptors for artificial memory erasure. *Nat Biotechnol*, in press.
51. Pryce CR, Bettschen D, Feldon J (2001) Comparison of the effects of early handling and early deprivation on maternal care in the rat. *Dev Psychobiol* 38(4):239–251.
52. Myers MM, Brunelli SA, Squire JM, Shindeldecker RD, Hofer MA (1989) Maternal behavior of SHR rats and its relationship to offspring blood pressures. *Dev Psychobiol* 22(1):29–53.
53. Rapaport PM, Maier SF (1978) Inescapable shock and food-competition dominance in rats. *Anim Learn Behav* 6(2):160–165.
54. Kroener S, et al. (2012) Chronic alcohol exposure alters behavioral and synaptic plasticity of the rodent prefrontal cortex. *PLoS One* 7(5):e37541.
55. Harris KM, Jensen FE, Tsao B (1992) Three-dimensional structure of dendritic spines and synapses in rat hippocampus (CA1) at postnatal day 15 and adult ages: Implications for the maturation of synaptic physiology and long-term potentiation. *J Neurosci* 12(7): 2685–2705.
56. Shin E, et al. (2013) Doublecortin-like kinase enhances dendritic remodelling and negatively regulates synapse maturation. *Nat Commun* 4:1440.